

EVALUATION OF PHYSIOCHEMICAL AND ELECTROCHEMICAL BEHAVIOUR OF REDUCED GRAPHENE FUNCTIONALIZED COPPER NANOSTRUCTURE AS AN EFFECTIVE CORROSION INHIBITOR

Haewon Byeon¹, K. Haribabu², Giriraj Kiradoo³, V.S. Sreenivasan⁴, M. Sivaprakash⁵, S. Richard⁶ and J. Sunil^{7*}

¹College of AI Convergence, Inje University, Gimhae, 50834, Republic of Korea

²Department of Mechanical Engineering, SCAD College of Engineering and Technology, Cheranmahadevi, Tirunelveli District- 627414, Tamil Nadu, India

³Engineering College Bikaner, Bikaner, Rajasthan, India

⁴Department of Mechanical Engineering, Sri Krishna College of Technology, Coimbatore - 641042, Tamil Nadu, India

⁵Department of Mechanical Engineering, Stella Mary's College of Engineering, Aruthenganvilai, Tamil Nadu 629202, India

⁶Department of Mechanical Engineering, Grace College of Engineering, Thoothukudi - 628 005, Tamil Nadu, India

⁷Department of Mechanical Engineering, Annai Vailankanni College of Engineering, Kanyakumari, India

(Received September 15, 2023; Revised November 3, 2023; Accepted November 9, 2023)

ABSTRACT. This study examines the physicochemical properties and corrosion resistance of hydrothermally produced copper oxide-reduced graphene oxide nanocomposite (CuO/rGO). The CuO/rGO nanocomposite has a well-defined and homogeneous structure, decreased crystal size, and uniformly distributed CuO nanoparticles tethered to the rGO. X-Ray diffraction confirms the fabrication of 15.1 nm crystalline monoclinic CuO nanoparticles. EDX confirms the composite's composition by detecting Cu, O, and C components. Electrochemical impedance spectroscopy (EIS) and potentiodynamic polarization (LSV) tests evaluate the CuO/rGO nanocomposite's corrosion resistance. A mild steel plate under an HCl electrolyte with corrosion in the PPM ratio treats the nanocomposite-coated substrate. The composite's synergistic effect is assessed by comparing its corrosion performance to CuO/rGO concentrations in ppm. The corrosion resistance data demonstrate that the CuO/rGO composite improves with inhibitor concentrations of 0, 25, 50, 75, and 100 ppm. Adding rGO to the composite protects it and speeds up charge transfer, reducing corrosion and improving stability. The composite's synergistic effect of CuO and rGO provides excellent corrosion resistance regardless of concentration, making it a viable material for corrosion-prone applications. The research develops novel and effective anti-corrosion methods to preserve materials in the food, automotive, and large-scale energy industries.

KEY WORDS: CuO/rGO nanocomposite, Tafel plot, Corrosion protection, Surface analysis

INTRODUCTION

Corrosion, the degradation of metals via chemical or electrochemical interactions with their surroundings, is still a significant and cost-prohibitive problem in many fields [1]. Innovative and practical ways to reduce corrosion's damaging impacts on metal buildings, equipment, and infrastructure are required. Coatings and protective layers that may prolong the service life and improve the durability of metal substrates have received much attention due to the increased usage of sophisticated materials for anti-corrosion applications. Incorporating composites as anti-corrosion materials has attracted much interest because of the possibility of increased protective performance [2]. Among the emerging materials for anti-corrosion applications, the copper

*Corresponding author. E-mail: sunil0520@gmail.com

This work is licensed under the Creative Commons Attribution 4.0 International License

oxide/reduced graphene oxide (CuO/rGO) composite has garnered considerable interest due to its unique properties and potential for combating corrosion [3]. The CuO/rGO composite capitalizes on the mutually beneficial effects of copper oxide nanoparticles and reduced graphene oxide sheets to generate a multifunctional and highly effective anti-corrosion material. Copper oxide nanoparticles have inherent corrosion resistance, while reduced graphene oxide provides an impermeable barrier and a large surface area for increased protection [4]. Copper, known for its excellent electrical and thermal conductivity, malleability, and ductility, has found wide applications in industries such as electronics, infrastructure, and transportation. However, its vulnerability to corrosion under aggressive conditions necessitates the development of reliable anti-corrosion solutions. Reduced graphene oxide, a derivative of graphene, possesses remarkable mechanical strength, high surface area, and exceptional chemical stability, making it an ideal candidate for enhancing the properties of composites. Copper oxide nanoparticles can significantly enhance corrosion resistance when added to coatings or applied directly to metal surfaces [5].

Reduced graphene oxide (rGO) possesses several vital properties, making it a promising material for anti-corrosion applications [6]. Some properties include impermeability, chemical stability, high surface area, electrical conductivity, ease of synthesis and biocompatible. These properties contribute to its ability to enhance the corrosion resistance of metal surfaces when used as a coating or additive. Its unique characteristics make it a promising material for developing advanced, durable anti-corrosion coatings for various industrial applications. Due to its unique properties, the copper/reduced graphene oxide (CuO/rGO) composite is a promising material in anti-corrosion applications [7]. This composite leverages the beneficial characteristics of both copper and reduced graphene oxide to provide a practical and durable corrosion-resistant coating or material. For any nanocomposite material that performs well against corrosion, the synthesis process, dispersion, and substrate adherence must be optimized [8]. There are several ways of synthesizing copper oxide nanoparticles/reduced graphene oxide. Nanoparticles can be optimized for specific applications by controlling their size, shape, and surface characteristics through synthesis [9]. Here, we synthesized copper oxide and reduced graphene oxide (rGO) through hydrothermal technique. This study investigates the physicochemical properties and corrosion resistance performance of the CuO/rGO composite when coated on mild steel (MS) plates. To assess the composite's ability against corrosion under different concentrations of CuO/rGO, the MS plates are used as a proxy substrate. Acidic medium (HCl) resembles corrosive conditions in industrial settings. The physicochemical properties of the composite will be examined through scanning electron microscopy (SEM), X-ray diffraction (XRD) and Fourier-transform infrared spectroscopy (FTIR). Electrochemical techniques, including potentiodynamic polarization and electrochemical impedance spectroscopy (EIS), will be employed to evaluate the corrosion resistance performance of the composite-coated MS plates under different electrolyte conditions.

EXPERIMENTAL

Materials and reagents

From the Merck chemical company, pure graphite powder, hydrochloric acid (HCl, 36.0-38.0 wt%), hydrogen peroxide (H₂O₂, 30 wt%), sulfuric acid (H₂SO₄, 95-98 wt%), potassium permanganate (KMnO₄), phosphorus pentoxide (P₂O₅), potassium persulfate (K₂S₂O₈), and ethanol (C₂H₅OH, > 99). Without any additional purification, all of the chemical reagents were employed in their original form [6].

Preparation of reduced graphene oxide (rGO)

The modified Hummers' approach produced graphene oxide (GO) from graphite powder [10]. A typical approach used 160 mL sulfuric acid and 40 mL orthophosphoric acid (4:1) with 1.6 g

graphite. This mixture was agitated for three days after adding 9 g of KMnO_4 . The black reactant solution turned bright yellow after dropwise addition of H_2O_2 (30%). The GO was obtained by filtering and washing the solution in 1 M HCl and DI water. The collected GO was vacuum-dried at 80 °C for 12 hours. Reduced graphene oxide (rGO) and graphene oxide (GO) were produced using hydrazine hydrate. Ultrasound dissolved 100 mg of the GO in 100 mL DI water. After adding 1 mL of hydrazine hydrate, the mixture was heated at 100 °C for 24 hours. The suspension was centrifuged, DI water washed, and dried to make rGO powder.

Synthesis of CuO/rGO nanocomposite

Initially, 25 mg of rGO was dispersed in 50 mL of DI water using ultrasonication to prepare CuO/rGO nanocomposites. A second beaker had 0.43 g of $\text{CuCl}_2 \cdot 2\text{H}_2\text{O}$ dissolved in 5 mL of DI water. An aqueous solution containing 15 mL of ammonia was then added, and the mixture was magnetically agitated for roughly 30 min. The combination was gradually added to the ready rGO suspension, placed in a stainless-steel autoclave with Teflon lining and heated at 140 °C for 24 hours. The precipitate was separated by centrifugation and then washed repeatedly in ethanol and DI water to remove any remaining ions. It was then dried for 12 hours at 80 °C. This sample was identified as a nanocomposite of CuO and rGO [8].

Material characterization

An X-ray diffraction machine (XRD 3003 TT) was used to examine the crystal structure and phase of the CuO/rGO nanocomposites using monochromatic nickel-filtered Cu K radiation. Using a CARL ZEISS SUPRA 55 with an energy-dispersive X-ray analyzer (EDAX) attachment for the elemental analysis, field emission scanning electron microscopy (FESEM) was used. Using a JOEL JEM 2100 advanced HRTEM, high-resolution transmission electron microscopic (HRTEM) pictures were captured. A PerkinElmer Spectrum was used to record the Fourier transform infrared (FT-IR) spectra.

Electrochemical corrosion analysis

A desired amount of CuO/rGO nanocomposite was dissolved in 100 mL of 1 M HCl to provide a solution of 0, 25, 50, 75, and 100 PPM inhibitors before the electrochemical test. Corrosion parameters were measured using an electrochemical workstation (Autolab, Metrohm, Netherlands) and a conventional three-electrode cell setup. As a counter, reference, and working electrodes, platinum sheet, saturated calomel, and mild steel were employed. The working electrode was submerged in the corrosion inhibitor solution at a steady open circuit potential (OCP) for 30 minutes before each measurement. The electrochemical impedance spectroscopy (EIS) was subsequently accomplished by applying a five-mV sinusoidal AC perturbation between 105 and 10^{-2} Hz. At one mV/s, the potentiodynamic polarization measurement was completed. The electrochemical tests were carried out three times to improve the reproducibility of data. After the completion of electrochemical studies, the surface properties of mild steel in each inhibitor were analysed using scanning probe microscopy (Hysitron nanoindenter, Ti-700, USA) and scanning electron microscopy analysis. The elemental composition of the mild steel plate used in this study have 0.17, 0.20, 0.54, 0.16, 2.2 and 96.5% of the carbon, silicon, manganese, phosphorus, oxygen and iron, respectively.

RESULTS AND DISCUSSION

The XRD diffractograms of the developed CuO/rGO nanocomposite are shown in Figure 1. By identifying its characteristic peaks in the CuO/rGO nanocomposite's XRD patterns, the CuO

phase's inclusion inside the produced nanocomposites is confirmed [11]. The CuO/rGO nanocomposite's reported XRD patterns were consistent with past reports, and the accepted JCPDS card no. 80.1916 [12].

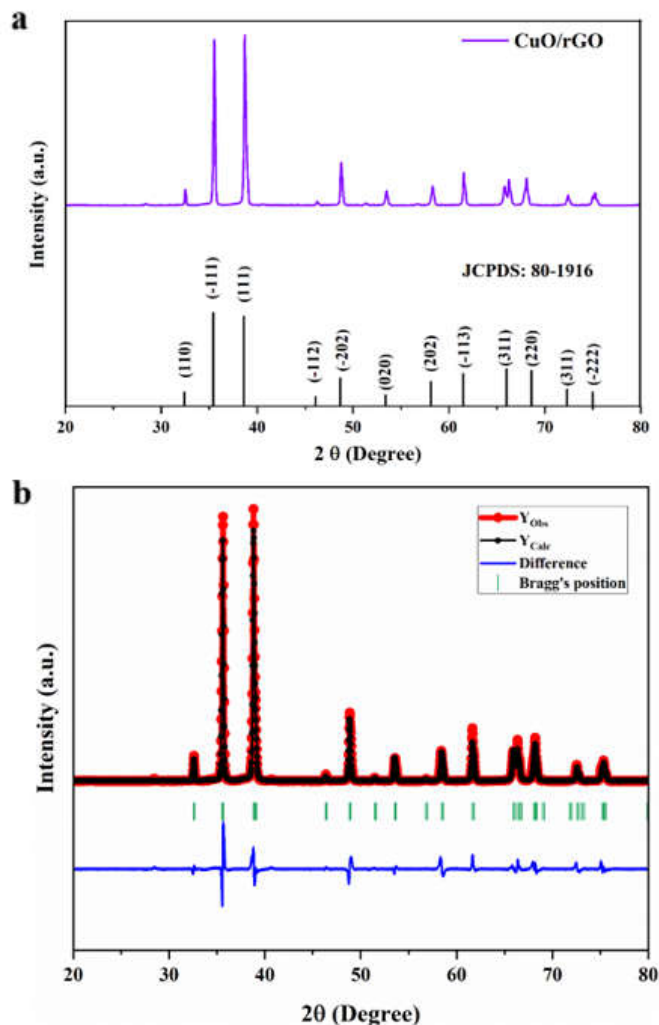


Figure 1. a) XRD pattern of CuO/rGO nanocomposite, b) refinement profile of CuO/rGO nanocomposite.

Additionally, the broad peaks that characterize CuO confirm that the substance is present as crystalline particles. The observed diffraction peaks are at 32.40, 35.42, 38.63, 46.10, 48.69, 53.40, 58.13, 62, 66, 67.89, 68.6, and 72.29 and their corresponding hkl values are (100), (-111), (111), (-112), (-202), (020), (202), (-113), (311), (220), and (-222), respectively for CuO/rGO nanocomposite whereas the (002) plane refers the rGO in nanocomposites. The rGO peak in XRD is small and practically buried. Figure 2 indicates that adding rGO to nanocomposites does not

influence CuO nanoparticle XRD patterns which was verified by earlier observations of pure CuO nanoparticles [13]. XRD signals in Figure 1a show that CuO/rGO nanocomposite was synthesized with great purity. The X-ray data of the obtained samples was Rietveld refined using the FULLPROF suite software [14]. The Rietveld refinement of room-temperature X-ray diffraction patterns for CuO/rGO nanocomposites is shown in Figure 1b. The significant structural parameters and Rietveld refinement details of CuO/rGO nanocomposite such as structural phase, space group, crystal size, dislocation density, micro strain and lattice parameters are monoclinic, C_2/c , 15.1 nm, $4.3 \times 10^{-3} \text{ nm}^{-2}$, 0.49% and 0.44, respectively. The FT-IR spectra of CuO/rGO are depicted in Figure 2. Due to physically adsorbed water, the broad absorption peaks at $3300\text{--}3600 \text{ cm}^{-1}$ are assigned to the O-H stretching [15]. C=O, C-H, and C-O are responsible for the faint peaks at 1632, 1469, and 1384 cm^{-1} , respectively. This suggests that heat treatment destroyed most of the oxygen-containing groups throughout the nanocomposites' production process [16]. The reduction of GO to rGO sheets is suggested by the bands at 1151 cm^{-1} , which can be attributed to the skeletal vibrations of C=C from graphitic domains. The vibrations of the Cu-O bonds are thought to cause firm absorption peaks at 649, 531, and 420 cm^{-1} . These findings support the synthesis of the CuO/rGO nanocomposite [17]. The two sharp peaks at 2854 and 2925 cm^{-1} are attributed to O-H stretching bond due to moisture or water molecules adsorbed on the surface of the prepared nanocomposites from the environment [18].

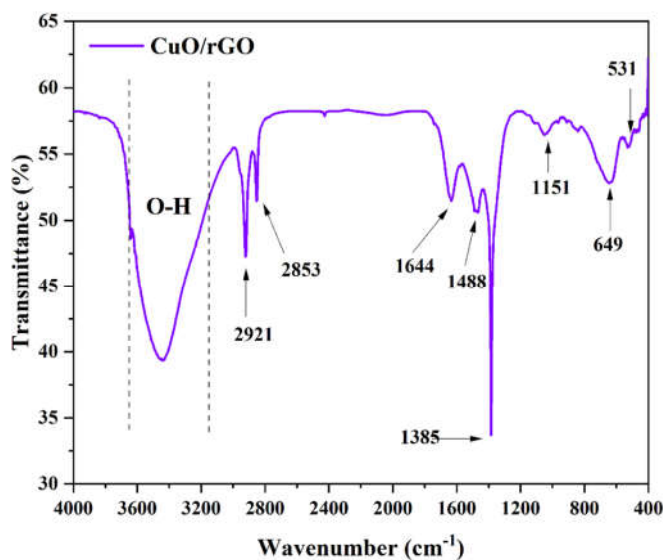


Figure 2. FTIR spectra of CuO/rGO nanocomposite.

Analyses of the morphologies of the as-synthesized CuO/rGO nanocomposites were performed using FESEM images, and examples of the morphological pictures are presented in Figure 3. As rough agglomerates, the spherical morphology of CuO nanoparticles may be seen, indicates that during the synthesis process, i.e., reaction time and temperature are altering the size of created CuO/rGO nanocomposites as they were growing.

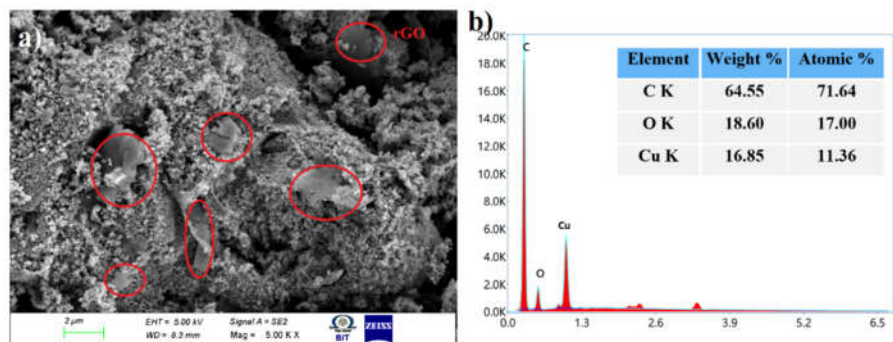


Figure 3. a) FESEM image and b) EDX spectra of CuO/rGO nanocomposite.

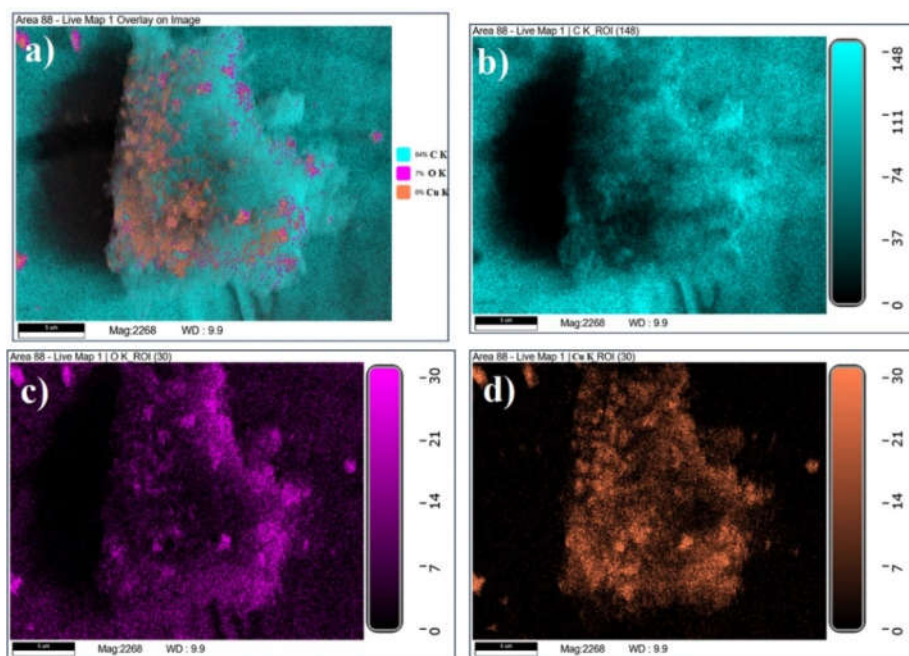


Figure 4. Elemental mapping analysis of CuO/rGO nanocomposite.

The morphology of reduced GO showed less evidence of aggregation, and individual sheets showed that the amount of GO had been reduced. The gradual change in morphology that occurred after adding CuO nanoparticles to rGO is consistent with the idea that the CuO nanoparticles bound with the rGO. As we compared with the morphology of the pure CuO nanoparticles from the earlier reports, the prepared samples have tiny grain sizes and uniformly distributed spherical morphology. This should happen due to the synthesis process and ammonia as reducing and stabilizing agents [19]. The energy dispersive X-ray examination (EDX) performed on the prepared sample revealed that the CuO/rGO nanocomposite did not include any impurities and

only included copper, carbon, and oxygen components. Figure 3b displays the EDX spectrum, and the table in the figure's insert outlines the elemental makeup of the sample about the desired ions. In addition, Figure 4 shows the elemental mapping images clearly show the distribution of Cu ions over rGO and wrapped over the sample. This homogeneous dispersal of CuO nanoparticles on rGO sheets was also confirmed from EDX spectra and mapping analysis.

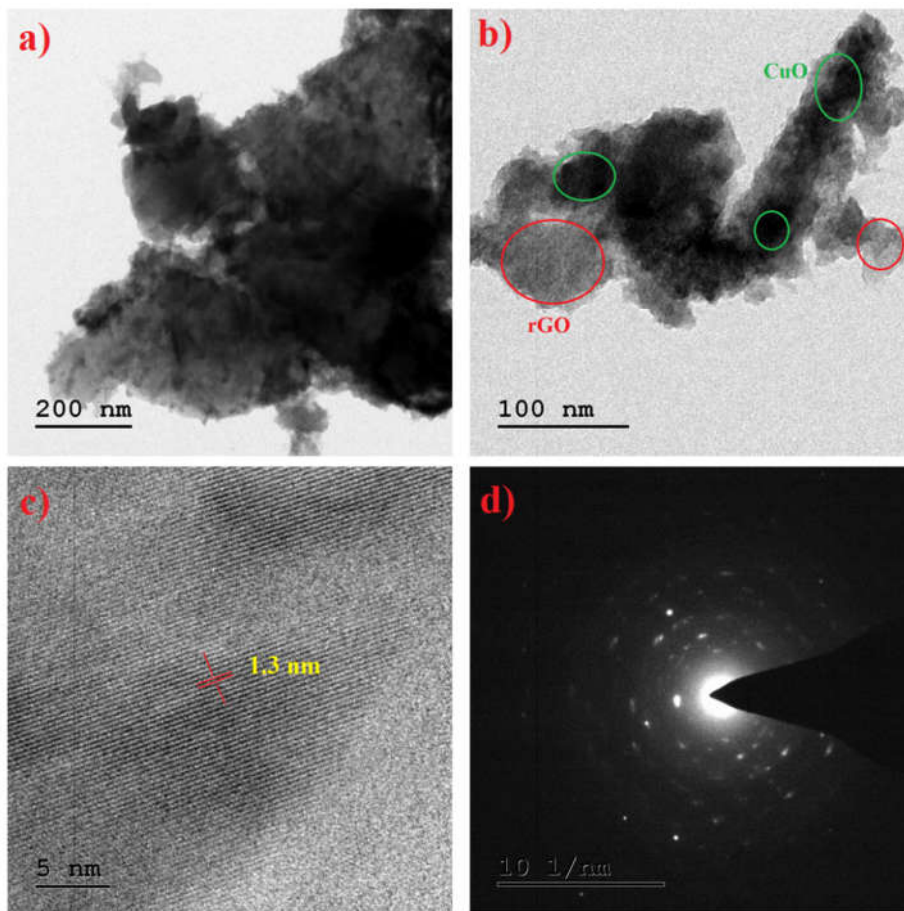


Figure 5. a) TEM image and b) SAED pattern of CuO/rGO nanocomposite.

The produced CuO/rGO nanocomposite's shape and structure were identified via HRTEM investigation. Figure 5 displays SAED patterns and HRTEM pictures of CuO/rGO. The photos demonstrate the presence of rGO particles and small, spherical CuO nanoparticles explicitly created to make giant spheres. In some areas of the HRTEM image of rGO, it may be possible to see the development of a sheet-like morphology with wrinkles and entangled structures. The CuO nanoparticles on the rGO sheets were uniformly distributed according to the HRTEM pictures of the CuO/rGO nanocomposite. The inset of each TEM image shows the samples' individually selected area electron diffraction (SAED) patterns as-made. The results of the XRD, FESEM,

and TEM analyses back up the conclusion that the produced sample had an average particle size as measured.

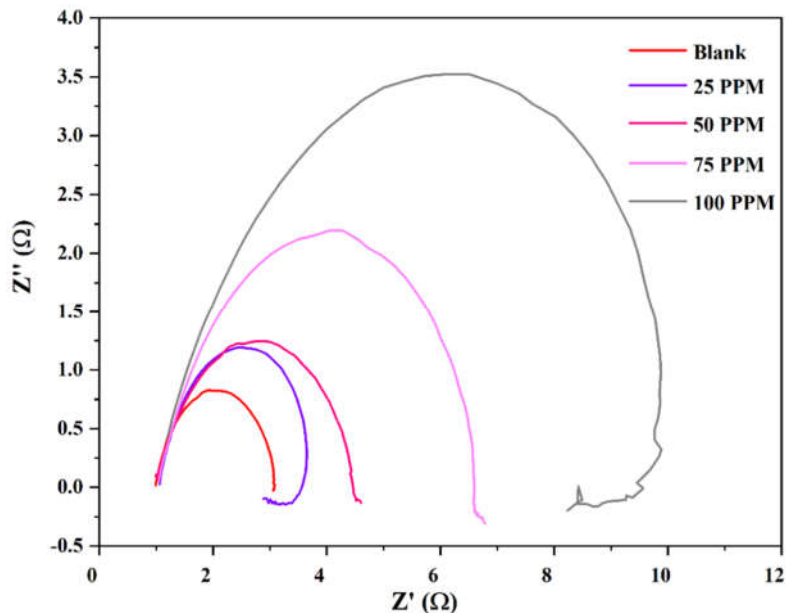


Figure 6. Electrochemical impedance spectra (Nyquist plot) of CuO/rGO nanocomposite.

Figure 6 shows the electrochemical impedance spectra (EIS) data. Due to adsorbed species on the mild steel plate's surface, Nyquist curves showed expanded capacitive loops after introducing the inhibitor. The direct correlation between the capacitive loop's diameter and inhibitor concentration suggests that many inhibitors might significantly suppress an aggressive solution's attack. The Nyquist figure displays a large capacitive loop at high frequencies (HF) and a modest inductive loop at low frequencies (LF) for the mild steel plate in 1 M HCl solution. The charge transfer mechanism at the electrode/solution interface is blamed for the HF capacitive loop, while the relaxation of Cl^- and H^+ ions on the MS metal substrate is thought to cause the LF inductive loop. However, compared to a control HCl solution, the shape of the Nyquist plots in the presence of CuO/rGO nanocomposite is different. This was explained by the fact that more inhibitors could cover the corrosion area before forming an adsorption film on the steel surface, giving them an excellent ability to block corrosion. Additionally, all Nyquist curves had comparable shapes, showing that adding the inhibitor improved the impedance value but did not affect the corrosion system's other electrochemical properties [22]. The measured impedance parameters of the mild steel in the presence of CuO/rGO nanocomposite are shown in Table 1. According to the findings in Table 1, as the concentration of CuO/rGO nanocomposite in 1 M HCl solution increases, the R_p value rises while C_{dl} falls. The development of an absorption layer at the metal/solution interface is thought to be responsible for the increase in R_p value and the decrease in C_{dl} . Adsorbed inhibitor film can enhance the double layer thickness or replace water molecules with inhibitor molecules at the mild steel/solution interface, lowering C_{dl} values. The most considerable inhibiting effect is observed at 100 PPM of CuO/rGO, giving an R_p value of 10.176 Ω higher than any other samples. The polarization resistance values of the mild steel are 4.2703, 1.9293, 3.8225, and 4.1388 Ω , respectively, for 0, 25, 50, 75 and 100 ppm. The increase in the peak heights with increasing concentrations of CuO/rGO nanocomposite at the ppm level implies

a more capacitive response at the metal-solution interface owing to the absorption of inhibitor molecules than other samples [23].

Table 1. Electrochemical impedance parameters of CuO/rGO nanocomposite.

Concentration	R_s (Ω)	R_p (Ω)	Cdl (mF)
Blank	1.09420	4.27030	9.9831
25 ppm	1.05090	1.92930	2.8916
50 ppm	691.440 m	3.82250	2.0243
75 ppm	1.41310	4.13880	1.1904
100 ppm	950.800 m	10.1760	1.0514

The results of the Tafel curves are shown in Figure 7. The addition of inhibitors caused the Tafel curves to shift away from the anode toward the cathode compared to the blank solution (0 ppm, 1 M HCl), and this behaviour became more prominent as the inhibitor concentration increased.

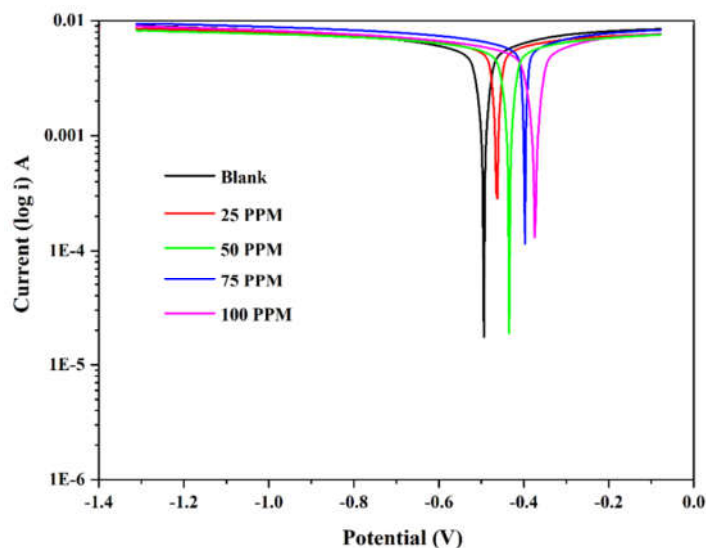


Figure 7. Potentiodynamic polarisation curves of CuO/rGO nanocomposite.

In addition, every Tafel curve generated by the inhibitor solutions had a cathode component parallel to the one generated by the blank solution. This demonstrated that the influence of the corrosion inhibitor on the cathode reaction mechanism was negligible. When steel was submerged in 50 ppm and 100 ppm solutions, a clear saltation around -1.21 V was seen in the anode part of Tafel curves (Figure 7), suggesting that the primary source of the adsorption essence was CuO/rGO nanocomposite [24]. The obtained potentiodynamic polarisation parameters are given in Table 2. Observationally, the i_{corr} value fell as inhibitor concentration was added to the HCl solution, showing a similar tendency to change in inhibition efficiency. Meanwhile, the i_{corr} value was negatively correlated with the inhibitor concentration, indicating that raising the inhibitor concentration in 1 M HCl significantly reduced mild steel corrosion. Calculations revealed that 100 ppm inhibitor solutions values were 14.12%, 23.06%, 57.66%, and 84.72%, respectively, for 25, 50, 75 and 100 ppm. This indicated that the CuO/rGO nanocomposite possessed excellent inhibition performance. The prepared inhibitor's corrosion inhibition properties have been

compared with various metal oxides and electrolytes, as shown in Table 3. When compared to other types of nanocomposites, the inhibitory efficiency of the CuO/rGO nanocomposite was higher. Additionally, the fluctuation of b_a and b_c values showed an upward trend compared to the control specimen, showing that the CuO/rGO nanocomposite was a mixed-type inhibitor capable of inhibiting both cathodic and anodic processes [25].

Table 2. Potentiodynamic polarisation parameters of CuO/rGO nanocomposite.

Inhibitor	E_{corr} (mV)	I_{corr} (A/cm ²)	Polarization resistance (Ω)	Corrosion rate (mm/year)	Improved corrosion resistance (%)
Blank	466.17	1.7709	4.36450	20.578	
25 ppm	457.05	1.5208	3.76940	17.672	14.12
50 ppm	472.63	1.3625	6.14460	15.832	23.06
75 ppm	465.59	921.84 μ	6.98120	8.7127	57.66
100 ppm	461.21	614.79 μ	7.39450	3.1438	84.72

Table 3. An assessment of nanoparticles as corrosion inhibitors under acidic conditions.

Substrate	Electrolyte	Inhibitor	Concentration (ppm)	Inhibition efficiency (%)
Steel	H ₂ SO ₄	Ag-chitosan	1000	93.09
Mild steel	0.5 M HCl	Ag NPs	20 (μ g/mL)	99.59
SS plate	1 M HCl	Ag NPs	20 (μ g/mL)	99.06
Al	1 M HCl	Ag NPs	20 (μ g/mL)	96.10
Carbon steel	1 M HCl	CoO/Co ₃ O ₄	80	91
Mild steel	0.5 M HCl	ZnO NPs	1x10 ⁻³ g	92
ST37 Steel	15% HCl	Ag/chitosan	1000	97.09
Carbon Steel	3.5% NaCl	N-S-CDs	50 (mg/L)	93
Mild steel	1 M HCl	CuO/rGO	100	84.72

The findings of the LSV tests revealed that the values of the coated plates' hardness and roughness had somewhat increased after being subjected to the coating. Throughout the electrochemical analysis, it was observed that the CuO/rGO inhibitor offered a sizeable amount of protection to the MS plate's surface. On the other hand, it was discovered that the surfaces of the MS plate sustained severe damage when subjected to a blank HCl solution [22]. The CuO/rGO composite, distinguished by its enormous surface area and excellent stability, promoted the rapid diffusion of ions from caustic electrolytes, including Cl and H ions. This was made possible by the wide surface area of the CuO/rGO composite.

CONCLUSION

The corrosion of mild steel in 1 M HCl with and without CuO/rGO nanocomposite solution could be prevented by forming a protective layer on the surface area. Moreover, the prepared nanocomposite showed high inhibitive efficiency for mild steel in 1 M HCl solution. The principal conclusions are emphasized as follows: (i) Feasible and effective hydrothermal method produced high crystalline and pure CuO/rGO nanocomposites for the best surface protection from corrosive agents. The structural and morphological optical properties are elaborately studied through various techniques and compared with earlier reports in detail. (ii) Based on the polarization measurements (LSV and Tafel) and EIS analysis results, CuO/rGO nanocomposite could effectively inhibit mild steel in 1 M HCl solution. Moreover, the inhibition efficiency was proportional to the concentration in the HCl solution. The maximum inhibition efficiency was achieved for 100 ppm concentration. (iii) According to the results, the corrosion inhibition of

CuO/rGO is due to the layer formation on the MS plate during the electrochemical process. This process looks like the coating method, namely the electrochemical deposition process. Also, metal surfaces are highly protected from aggressive agents, which could lead to less damage. (iv) Overall, the reduced graphene oxide highly encourages the surface protection properties of CuO nanoparticles by making composite with them.

FUNDING

This research Supported by Basic Science Research Program through the National Research Foundation of Korea (NRF) funded by the Ministry of Education (NRF- RS-2023-00237287, NRF-2021S1A5A8062526) and local government-university cooperation-based regional innovation projects (2021RIS-003).

REFERENCES

- Hanifah, I.R.; Sofyan, N. Reduced graphene oxide synthesized from bamboo for mild steel anti-corrosion coating in saline water. *AIP Conf. Proc.* **2023**, *1*, 153–165.
- Liu, Z.; Zhu, R.; Zhang, X.; Zhu, H. Improving anti-corrosion performance of epoxy coating by hybrids of rGO and G-C3N4 nanosheets. *J. Coat. Technol. Res.* **2022**, *19*, 1219–1232.
- Bordbar-Khiabani, A.; Ebrahimi, S.; Yarmand, B. Highly corrosion protection properties of plasma electrolytic oxidized titanium using rGO nanosheets. *Appl. Surf. Sci.* **2019**, *486*, 153–165.
- Dehghani, A.; Bahlakeh, G.; Ramezanzadeh, B.; Hossein Jafari Mofidabadi, A. 2D reduced-graphene oxide (rGO) nanosheets decorated with l-histidine loaded- β -cyclodextrin for efficient epoxy nanocomposite anti-corrosion properties; DFT-D modeling/experimental assessments. *Flat. Chem.* **2021**, *30*, 100309.
- Dehghani, A.; Hossein Mostafatabar, A.; Bahlakeh, G.; Ramezanzadeh, B. Poppy-leaf extract-derived biomolecules adsorption on the rGO-nanoplatfoms and application as smart self-healing material for epoxy coating. *J. Mol. Liq.* **2023**, *370*, 120931.
- Cuong, H.N.; Pansambal, S.; Ghotekar, S.; Oza, R.; Thanh Hai, N.T.; Viet, N.M.; Nguyen, V.-H. New frontiers in the plant extract mediated biosynthesis of copper oxide (CuO) nanoparticles and their potential applications: A review. *Environ. Res.* **2022**, *203*, 111858.
- Hong, L.; Wang, L.-Y.; Wang, Y.; Wu, X.; Huang, W.; Zhou, Y.; Wang, K.-X.; Chen, J.-S. Toward hydrogen-free and dendrite-free aqueous zinc batteries: Formation of zincophilic protective layer on Zn anodes. *Adv. Sci.* **2022**, *9*, e2104866.
- Han, G.; Marimuthu, K.P.; Lee, H. Evaluation of thin film material properties using a deep nanoindentation and ANN. *Mater. Des.* **2022**, *221*, 111000.
- Chauhan, A.; Verma, R.; Batoo, K.M.; Kumari, S.; Kalia, R.; Kumar, R.; Hadi, M.; Raslan, E.H.; Imran, A. Structural and optical properties of copper oxide nanoparticles: A study of variation in structure and antibiotic activity. *J. Mater. Res.* **2021**, *36*, 1496–1509.
- Luna, I.Z.; Hilary, L.N.; Chowdhury, A.M.S.; Gafur, M.A.; Khan, N.; Khan, R.A. Preparation and characterization of copper oxide nanoparticles synthesized via chemical precipitation method. *OAlib* **2015**, *02*, 1–8.
- Thakar, M.A.; Saurabh Jha, S.; Phasinam, K.; Manne, R.; Qureshi, Y.; Hari Babu, V.V. X-Ray diffraction (XRD) analysis and evaluation of antioxidant activity of copper oxide nanoparticles synthesized from leaf extract of *Cissus vitiginea*. *Mater. Today: Proceedings* **2022**, *51*, 319–324.
- Lanje, A.S.; Sharma, S.J.; Pode, R.B.; Ningthoujam, R.S. Synthesis and optical characterization of copper oxide nanoparticles. *Adv. Appl. Sci. Res.* **2010**, *1*, 36–40.
- Yang, W.; Feng, W.; Liao, Z.; Yang, Y.; Miao, G.; Yu, B.; Pei, X. Protection of mild steel with molecular engineered epoxy nanocomposite coatings containing corrosion inhibitor functionalized nanoparticles. *Surf. Coat. Technol.* **2021**, *406*, 126639.

14. Roisnel, T.; Rodríguez-Carvajal, J. Laboratoire Léon Brillouin (CEA/CNRS), CEA-Saclay 91191, **2001**.
15. Jain, P.; Patidar, B.; Bhawsar, J. Potential of nanoparticles as a corrosion inhibitor: A review. *J. Bio- and Tribo-Corrosion* **2020**, *6*, 43.
16. Raja, P.B.; Sethuraman, M.G. Natural products as corrosion inhibitor for metals in corrosive media — a review. *Mater. Lett.* **2008**, *62*, 113–116.
17. Liu, C.; Qiu, S.; Du, P.; Zhao, H.; Wang, L. An ionic liquid–graphene oxide hybrid nanomaterial: Synthesis and anti-corrosive applications. *Nanoscale* **2018**, *10*, 8115–8124.
18. Zheng, S.; Bellido-Aguilar, D.A.; Huang, Y.; Zeng, X.; Zhang, Q.; Chen, Z. Mechanically robust hydrophobic bio-based epoxy coatings for anti-corrosion application. *Surf. Coat. Technol.* **2019**, *363*, 43–50.
19. Jiang, F.; Zhao, W.; Wu, Y.; Wu, Y.; Liu, G.; Dong, J.; Zhou, K. A Polyethyleneimine-grafted graphene oxide hybrid nanomaterial: Synthesis and anti-corrosion applications. *Appl. Surf. Sci.* **2019**, *479*, 963–973.
20. Sudha, M.; Surendhiran, S.; Gowthambabu, V.; Balamurugan, A.; Anandarasu, R.; Syed Khadar, Y.A.; Vasudevan, D. Enhancement of corrosive-resistant behavior of Zn and Mg metal plates using biosynthesized nickel oxide nanoparticles. *J. Bio- and Tribo-Corrosion* **2021**, *7*, 60.
21. Ravikumar, S.; Surendhiran, S.; Sunil, J.; Suresh, K.C.; Balamurugan, A.; Khadar, Y.A.; Benham, A. Facile and Scalable Synthesis of ZnS and Tin Doped ZnS Nanostructures: A Study on Electrochemical Properties for Corrosion Applications in Proceedings of the AIP Conference Proceedings. *AIP Conf. Proc.* **2022**, *2385*, 020001.
22. Khadar, Y.A.S.; Surendhiran, S.; Gowthambabu, V. Enhancement of corrosion inhibition of mild steel in acidic media by green-synthesized nano-manganese oxide. *Mater. Today Proc.* **2021**, *47*, 889-893.
23. Kavitha, V.; Mayandi, J.; Mahalingam, P.; Sethupathi, N. Structural, optical and electrical studies on zinc doped barium strontium titanate as photo-anode for DSSC device. *Mater. Today Proceedings* **2021**, *35*, 48–52.
24. Kandasamy, K.; Surendhiran, S.; Jagan, K.S.G.; Kumar, G.S.; Khadar, Y.A.S.; Rajasingh, P. Green synthesis of CdS quantum dots for photocatalytic and anti-corrosive applications in aqueous media. *Appl. Surface Sci. Adv.* **2023**, *13*, 100364.
25. Liu, Z.; Zhu, R.; Zhang, X.; Zhu, H. Improving anti-corrosion performance of epoxy coating by hybrids of rGO and G-C3N4 nanosheets. *J. Coat. Technol. Res.* **2022**, *19*, 1219–1232.